CHAPTER IV

RESULTS AND DISCUSSION

1. Study of Isolation methods of oxyresveratrol from the heartwood of *Artocarpus lakoocha*

1.1 Extraction

The study was initiated to find an extraction procedure that is appropriate for large-scale isolation of oxyresveratrol from *A. lakoocha*. Three different organic solvents, i.e. EtOH, acetone and EtOAc, were chosen as the dissolving media. MeOH was not used due to possible toxicity to humans. Five different extraction methods, including reflux, soxhlet, sonication, 8-hr maceration and 48-hr maceration were employed. The reflux and soxhlet methods are heat-assisted operations whereas the sonication and maceration methods are usually carried out at ambient temperature. From Table 3, It can be seen that the Soxhlet extraction method gave the most extracting power yielding the highest weight of extract regardless of the kind of organic solvent. EtOH was found to be the strongest solvent in all extraction methods. HPLC analysis of the oxyresveratrol content in each extract indicated that the EtOH extract obtained by the soxhlet method contained the highest amount of oxyresveratrol (6% based on the dried weight of heartwood) (Table 3). Comparison of the HPLC chromatograms of all of the extracts obtained by different extraction procedures (Figure 6) revealed that they all shared similar chromatographic patterns with only slight differences. It appeared that among the extraction procedures tested in this study, the Soxhlet extraction with EtOH method was the most productive.

1.2 Separation of the EtOH extract

The vacuum liquid chromatographic (VLC) method was chosen for the study because of its known efficiency and feasibility. It usually gives a quick separation with fair to good resolution depending on the nature of the sample and the types of stationary

phase and mobile phase. The instruments required for the technique are also widely available, including in the Pharmacognosy laboratory. Although open column chromatography is a more simple method, the flow of the mobile phase is normally much slower and large quantities of solvent are usually consumed. High performance liquid chromatography (HPLC) and related techniques such as MPLC and LPLC require sophisticated instruments and may possess high separation power, but are not suitable for the industrial scale isolation of oxyresveratrol. As for the separation methods concerning the difference of partition coefficients of the constituents in the extract, several preliminary studies using H_2O paired with an organic solvent such as CH_2Cl_2 and EtOAc did not give clear-cut distribution of oxyresveratrol.

For the VLC in this study, commercially available adsorbents, i.e. silica gel, aluminium oxide and kieselguhr were used. Elution was performed with a gradient of CH_2Cl_2/EtOH (Table 4). From the appearance of the TLC chromatograms (Figure 5) together with the weights of the obtained fractions (Tables 5-7), it appeared that under the same condition, aluminium oxide gave the highest yield of oxyresveratrol, as well as the best resolution, although the thickness of adsorbent was thinnest. For silica gel, oxyresveratrol appeared to degrade quickly, as seen from the yellow materials which gradually appeared on the adsorbent during the isolation process. This phenomenon was not observed in the case of aluminium oxide or kieselguhr. Kieselguhr, however, gave poor resolution as judged from the TLC chromatogram and the weights of fractions containing oxyresveratrol.

1.3 Isolation of oxyresveratrol from Puag-Haad by MPLC

MPLC was used to isolate oxyresveratrol from Puag-Haad. The fractions received were clear and gave high yields of pure oxyresveratrol up to fifty percent. But it took a long period per isolation (6-8 hours). Therefore, this method does not practical enough for large scale production. As a result this method was used to prepare pure compound for standard oxyresveratrol.

1.4 Purification

Purification of crude oxyresveratrol obtained from chromatographic fractions was studied by attempting recrystallization from MeOH, EtOH or acetone. In all methods, colorless needles were obtained with no observable physical difference. However, yellow color developed quickly on the surface of the crystals if the sample was not readily dried or was strongly exposed to heat or light. Oxyresveratrol was found to have low solubility in EtOAc and CH_2Cl_2.

2. Analytical method for determination of oxyresveratrol in extracts and Puag-Haad

Since oxyresveratrol has a wide range of potential applications in the pharmaceutical, cosmetic and food industry, there appears a need for a reliable analytical method for the detection of oxyresveratrol in matrixes. Prior to this investigation, no analytical methods for analyzing oxyresveratrol in plant extracts or plant products have been reported. In this study, development of a simple high performance chromatographic (HPLC) analytical method was attempted. A reverse-phase C-18 column was used, and isocratic elution was carried out with H_2O/MeOH as the mobile phase, both of which are inexpensive and widely available solvents. The retention time of oxyresveratrol was 5 min, indicating short operation time. Overall, it took about 15 min per run. A fair to good resolution was also obtained depending on the nature of the sample. This analytical method was then validated on five parameters: accuracy, precision, linearity, limit of detection and limit of quantitation.

The accuracy was determined by recovery experiments. The study was carried out by adding oxyresveratrol with known varying amounts to a set of three sample solutions. A spike was detected on the HPLC chromatogram for each solution (Figure 7F). The quantity of added oxyresveratrol in each sample was determined using the standard curve and % recovery was calculated. In this study, the observed % recovery values were satisfactory, being in the range of 103.8 –110.5 %.

For the study of precision of the analytical method, repeatability experiments were conducted. Mean concentration of oxyresveratrol, along with standard deviation, was

determined from ten replicates using the standard curve, and the precision was calculated and expressed as relative standard deviation (RSD). For this analytical method, % RSD was found to be 1.22, which represented very good precision.

Linearity was readily determined from the standard curve obtained by plotting oxyresveratrol concentrations versus areas under curve (AUC S), which showed linear correlation with a coefficient of determination (r^2) = 0.998 for the equation —Y = $5x10^5X+623683$.

The limit of detection (LOD) of this analytical method was 0.0012 mg/ml (1.2 μg/ml), and the limit of quatitation (LOQ) was 0.004 mg/ml (4.0 μg/ml) as determined from the y axis-intercept of the line correlating SD and concentration.

Thus, based on the above data, the HPLC analytical method developed in this study appears to be a simple, reliable, fast and economical procedure which can be easily implemented in a standard analytical laboratory. It should be mentioned that the method was used for the determination of oxyresveratrol in extracts and Puag-Haad in this study. It is interesting to note that a very high content of oxyresveratrol (98%) was found in the sample of the traditional drug Puag-Haad .

3. Structural characterization of modified compounds

All of the structures of the modified compounds were characterized by analysis of their physical and spectral properties, including the UV, IR, NMR and MS data.

3.1. Structural characterization of oxyresveratrol tetra-ethylcarbonate (AS-1)

Compounds AS-1 was obtained as an oil. The UV spectrum (Figure 29) showed a maximal absorption at λ_{max} 297 nm, and exhibited IR bands (Figure 30) at 3285, 1756, 1215 and 998 cm^{-1}. The EI mass spectrum (Figure 31) revealed a $[M]^+$ ion at *m/z* 532, consistent with the molecular formula $C_{26}H_{28}O_{12}$. Other significant peaks were found at *m/z* 388 ($C_{10}H_{12}O_6$) and 226 ($C_{10}H_{12}O_6$). The high resolution mass spectroscopy revealed *m/z* at 533.1656 (533.1660 calculated for $C_{26}H_{29}O_{12}$).

The presence of the added four ethyl carbonate groups was confirmed by ^{1}H NMR signals of four methyl groups at δ1.38 (12 H, m) and four methylene groups at δ4.35 (8H, m). Eight proton signals were observed in the olefinic and aromatic regions. The ^{13}C NMR spectrum revealed the presence of methyl carbons at δ 14.9 and methylenes at δ 65.9 and 65.6. The carbonate carbonyl carbons appeared at δ 153.3, 153.4 and 153.5.

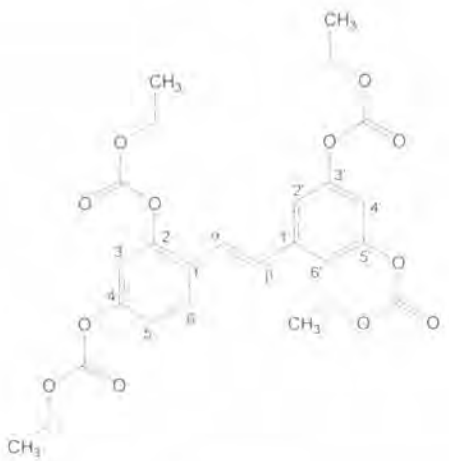

Figure 11: Structure of compound AS-1

3.2. Structural characterization of oxyresveratrol tetra-diethylcarbamate (AS-2)

Compounds AS-2 was obtained as a viscous oil. The UV spectrum (Figure 34) showed a maximal absorption at λ_{max} 299 nm, and exhibited IR bands (Figure 35) at 2974, 1710 and 1145 cm^{-1}. The EI mass spectrum (Figure 36) revealed a $[M]^{+}$ ion at *m/z* 640, consistent with the molecular formula $C_{34}H_{48}N_4O_8$. Other significant peaks were found at *m/z* 328 ($C_{17}H_{12}O_7$) and 286 ($C_{15}H_8O_5$). The high resolution mass spectroscopy revealed *m/z* at 641.3537 (641.3551 Calculated for $C_{34}H_{49}N_4O_8$)

The presence of four diethyl carbamate groups in compound AS-2 was confirmed by the ^{1}H NMR signals of eight methyl groups at δ 1.18 (24H, br s) and eight methylene protons at δ 3.37 (16H, br s). Signals for eight protons were found in the olefinic and aromatic regions. The ^{13}C NMR spectrum revealed the presence of four methyl carbons at δ 13.5, 14.4, eight methylene carbons at δ 42.0 and 42.3. The carbamate carbons showed at δ 153.4 and 153.6.

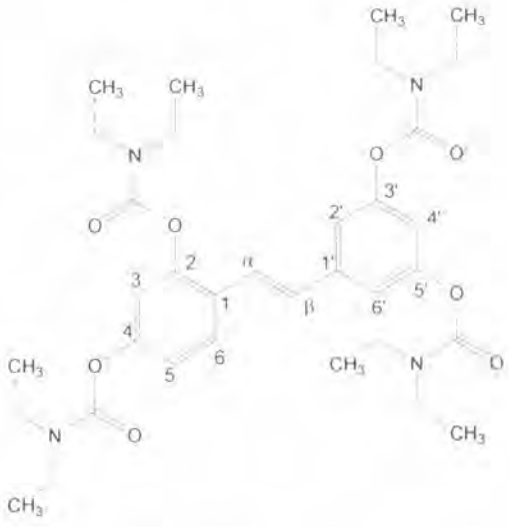

Figure 12: Structure of compound AS-2

3.3. Structural characterization of oxyresveratrol tetra-acetate (AS-3)

Compounds AS-3 was obtained as a yellow solid. The UV spectrum (Figure 39) showed a maximal absorption at λ_{max} 297 nm, and exhibited IR bands (Figure 40) at 3285, 1756, 1366 and 1192 cm^{-1}. The EI mass spectrum (Figure 41) revealed a $[M]^+$ ion at *m/z* 412, consistent with the molecular formula $C_{22}H_{20}O_8$. Other significant peaks were found at *m/z* 328 ($C_{18}H_{16}O_6$) and 286 ($C_{16}H_{11}O_5$). The high resolution mass spectroscopy revealed *m/z* at 413.1229 (413.1237 calculated for $C_{22}H_{21}O_8$).

The four acetyl groups of AS-3 appeared in the ^1H NMR spectrum at δ 2.34 (3H, s), 2.89 (6H, s) and 2.28 (3H, s). Six aromatic and two olefinic protons were observed. The ^{13}C NMR spectrum revealed the presence of methyl carbons in the acetyl groups at δ 21.2 and 21.1. In addition, the presence of ester carbons at δ 168.6 was observed. The other remaining carbon signals were similar to those of oxyresveratrol but appeared at more down field positions.

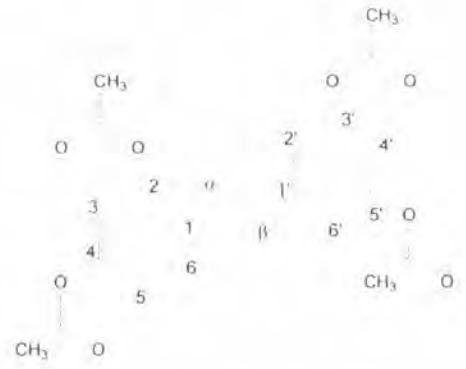

Figure 13: Structure of compound AS-3

3.4. Structural characterization of oxyresveratrol tetra-benzoate (AS-4)

Compounds AS-4 was obtained as a white solid. The UV spectrum (Figure 44) showed a maximal absorption at λ_{max}, 242 nm, and exhibited IR bands (Figure 45) at 1728 and 1259 cm^{-1}. The EI mass spectrum (Figure 46) revealed a $[M]^+$ ion at *m/z* 660, consistent with the molecular formula $C_{42}H_{28}O_8$. Other significant peaks were found at *m/z* and 368 ($C_{24}H_{16}O_4$). The high mass spectrum revealed a $[M]^+$ ion at *m/z* 661.1841 (661.1863 calculated for $C_{42}H_{29}O_8$).

Compound AS-4 showed twenty additional aromatic proton signals, confirming the presence of four benzoyl groups but complex and unresolved signals from 7.10-8.30. The ^{13}C NMR spectrum revealed the presence of four ester carbonyl carbons at δ 165.1 and 165.0.

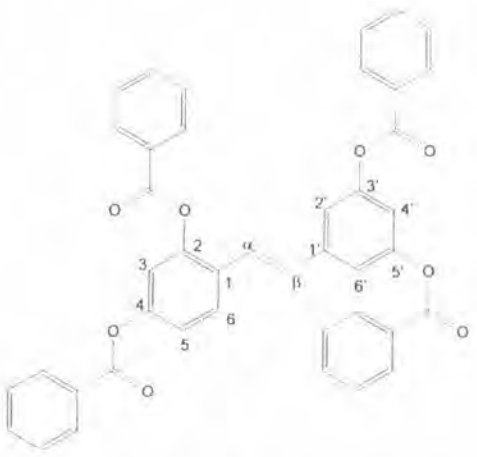

Figure 14: Structure of compound AS-4

3.5. Structural characterization of tetra-*O*-phenylmethyl oxyresveratrol (AS-5)

Compounds AS-5 was obtained as a white solid. The UV spectrum (Figure 49) showed a maximal absorption at λ_{max} 329 nm, and exhibited IR bands (Figure 50) at 1595, 1287 cm^{-1}. The high mass spectrum revealed a $[M]^+$ ion at *m/z* 605.2688 (found) 605.2692 (calculated for $C_{42}H_{37}O_4$).

The presence of four phenylethyl group in compound AS-5 was indicated by the ^1H NMR signals of four methylene groups at δ 5.09 (2H, s), 5.03 (6H, s). The proton signals in the olefinic and aromatic region were due to twenty eight protons. The ^{13}C NMR resonances at δ 71.1, 70.8 and 70.6 showed the presence of methylene carbons connected to the ether bridges.

Figure 15: Structure of compound AS-5

3.6. Structural characterization of tetra-*O*-methyl oxyresveratrol (AS-6)

Compounds AS-6 was obtained as a white solid from a methylation reaction by dimethyl sulfate or methyl iodide. The UV spectrum (Figure 53) showed a maximal absorption at λ_{max} 325 nm, and exhibited IR bands (Figure 54) at 2937 (OH) and 1587 (aromatic ring) cm^{-1}. The TOF mass spectrum (Figure 55) revealed a $[M+H]^+$ ion at *m/z* 301, consistent with the molecular formula $C_{18}H_{20}O_4$. Other significant peaks were found at *m/z* 199. The high resolution mass spectroscopy revealed *m/z* at 323.1263 (323.1262 calculated for $C_{18}H_{21}O_4$)

Compound AS-6 had a *trans*-configuration as indicated by the appearance of the two olefinic protons at δ 7.40 and 6.97 (J = 16.4 Hz). The presence of four methoxy proton groups were indicated by signals at δ 3.79 (3H, s), 3.77 (3H, s) and 3.62 (6H, s). Six aromatic protons appeared at δ 7.53 (1H, d, 8.6 Hz), 6.70 (2H, s), 6.54 (1H, d, 8.6 Hz), 6.50 (1H, br s) and 6.40 (1H, br s). The ^{13}C NMR spectrum revealed the presence of methoxyl carbons at δ 55.6, 55.5 and 55.4. The other carbon signals were similar to those of oxyresveratrol.

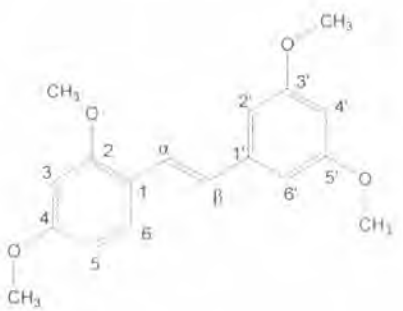

Figure 16: Structure of compound AS-6

3.7. Structural characterization of dihydrooxyresveratrol (AS-7)

Compounds AS-7 was obtained from hydrogenation reaction of oxyresveratrol as a pink-brown flake-like compound. The UV spectrum (Figure 58) showed a maximal absorption at λ_{max} 280 nm, and exhibited IR bands (Figure 59) at 3204 (OH) and 1519 (aromatic ring) cm^{-1}. The EI mass spectrum (Figure 60) revealed a $[M]^+$ ion at *m/z* 246, consistent with the molecular formula $C_{14}H_{14}O_4$. Other significant peaks were found at *m/z* 123 ($C_7H_7O_2$). The high resolution mass spectroscopy revealed *m/z* at 247.0962 (247.0971 calculated for $C_{14}H_{15}O_4$).

Compound AS-7 had two pairs of methylene protons at δ 2.55 (4H, m), instead of two olefinic protons as seen in oxyresveratrol. In addition, the presence of four OH groups was indicated by the signals at δ 9.09, 9.02 and 8.94. Six aromatic protons appeared at δ 6.78 (1H, d, J = 8.1 Hz), 6.25 (1H, d, J =1.7 Hz), 6.09 (1H, dd, J = 8.1, 1.7Hz), 6.05 (2H, br s) and 5.99 (1H, br s,). The ^{13}C NMR spectrum revealed the presence of two methylene carbons at δ 37.2 and 32.2.

Figure 17: Structure of compound AS-7

3.8. Structural characterization of 2,3′-di-O-methyl oxyresveratrol (AS-8)

Compounds AS-8 was obtained as a brown-yellow solid from partial methylation reaction using methyl iodide. The UV spectrum (Figure 63) showed a maximal absorption at λ_{max} 325 nm, and exhibited IR bands (Figure 64) at 3361 (OH) and 1589 (aromatic ring) cm^{-1}. The TOF mass spectrum (Figure 65) revealed a $[M]^+$ ion at *m/z* 272 ($C_{15}H_{12}O_3$), consistent with the molecular formula $C_{16}H_{16}O_3$. The high resolution mass spectroscopy revealed *m/z* at 273.1121 (273.1128 calculated for $C_{16}H_{17}O_3$).

The presence of two methoxy groups in compound AS-8 was confirmed by the ^1H NMR signals at δ 3.79 (3H, s) and 3.76 (3H, s). Two olefinic protons showed at δ 7.27 and 6.81 (1H each, d, 16.2 Hz), 6.37 (1H, br s), 6.39 (1H, br d, 8.4), 7.36 (1H, d 8.4), 6.55 (2H, br s) and 6.25 (1H, br s). The ^{13}C NMRspectrum revealed the presence of methoxy carbons at δ 55.5 and 55.3.

The positions of the methoxyl groups were determined from NOESY correlations as summarized in Figure 68.

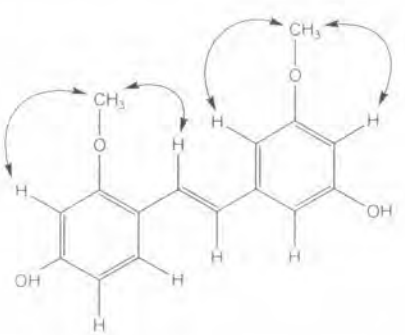

Figure 18: NOE interactions observed of compound AS-8

3.9. Structural characterization of 4,3′-di-*O*-methyl oxyresveratrol (AS-9)

Compounds AS-9 was obtained as a brown-yellow solid from partial methylation reaction of oxyresveratrol. The UV spectrum (Figure 69) showed a maximal absorption at λ_{max} 327 nm, and exhibited IR bands (Figure 70) at 3374 (OH) and 1515 (aromatic ring) cm^{-1}. The ESI mass spectrum (Figure 71) revealed a $[M]^+$ ion at *m/z* 272, suggesting the molecular formula $C_{16}H_{16}O_4$. Other significant peaks were found at *m/z* 254 ($C_{16}H_{15}O_3$). The high resolution mass spectroscopy revealed *m/z* at 295.0946 (295.0948 calculated for $C_{16}H_{16}O_4Na$).

Compound AS-9 contained two methoxyl groups, as indicated by the ^1H NMR signals at δ 3.79 (3H, s) and 3.78 (3H, s). The phenolics proton showed integration of eight protons, signal at δ 6.36 (1H, d, 2.4), 6.50 (1H, dd, 8.7, 2.4), 7.39 (1H,d, 8.7), 6.61(1H, br s), 6.30 (1H, t, 1.8), 6.58 (1H, br s), and the ^{13}C NMR resonances at δ 55.2 The positions of the methoxyl groups were established from the NOESY correlation peaks (Figure 74).

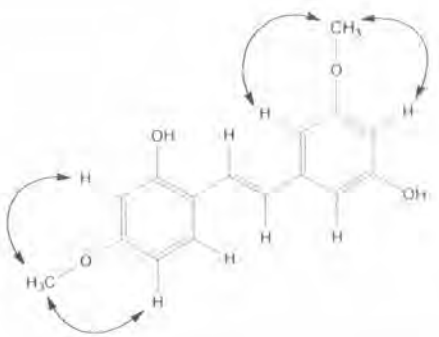

Figure 19: NOE interactions observed of compound AS-9

3.10. Structural characterization of 2-*O*-methyl oxyresveratrol (AS-10)

Compounds AS-10 was obtained as a brown-yellow solid from partial methylation. The UV spectrum (Figure 75) showed a maximal absorption at λ_{max} 326 nm, and exhibited IR bands (Figure 76) at 3331 (OH) and 1600 (aromatic ring) cm^{-1}. The mass spectrum (TOF) (Figure 77) revealed a $[M]^+$ ion at *m/z* 258, consistent with the molecular formula $C_{15}H_{14}O_4$. Other significant peaks were found at *m/z* 228 ($C_{14}H_{10}O_3$). The high

resolution mass spectroscopy revealed *m/z* at 281.0789 (281.0792 calculated for $C_{15}H_{14}O_4Na$).

Compound AS-10 possessed one methoxyl group, as evidenced by the ^1H NMR signal at δ 3.79 (3H, s) and the ^{13}C NMR signal at δ 55.7. The proton remains six with two olefinic protons. From the NOESY spectrum (Figure 80), NOE interaction was observed between H-3 and the methoxyl protons.

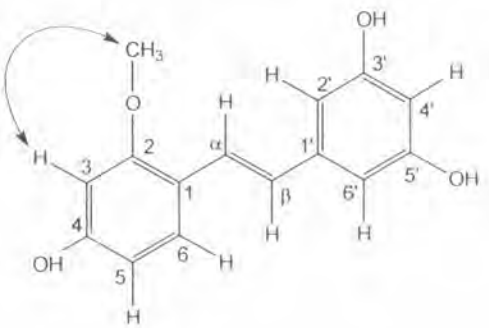

Figure 20: NOE interactions observed of compound AS-10

3.11. Structural characterization of 6-chloro-oxyresveratrol (AS-11)

Compounds AS-11 was obtained as a yellow-brown solid from chlorination reaction of oxyresveratrol. The UV spectrum (Figure 81) showed a maximal absorption at λ_{max} 218 and 332 nm, and exhibited IR bands (Figure 82) at 3375, 3286, 3187 (OH) and 1519. (aromatic ring), 1034, 1098 (chloroaromatic) cm^{-1}. The EI mass spectrum (Figure 83) revealed a $[M]^+$ ion at *m/z* 278, consistent with the molecular formula $C_{14}H_{12}ClO_4$. Other significant peaks were found at *m/z* 243 ($C_{14}H_8ClO_2$), 215 ($C_{13}H_{11}O_3$) and 197 ($C_{13}H_9O_2$). The $[M]^+$ ion at *m/z* 278, 243, 215 and 197 were three times higher than $[M+2H]^+$ ion which was the pattern of chlorinated compounds.

Compound AS-11 was confirmed of the presence of a chlorine atom by the high resolution mass spectrum which revealed a $[M+H]^+$ ion at *m/z* 279.0426 (calculated for $C_{14}H_{12}ClO_4$ 279.0425). Five aromatic protons appeared at δ 7.45 (1H, d, 8.5), 6.77 (1H, d, 3 Hz), 6.41 (1H, dd, 8.5, 2.5), 6.37 (1H, d, 3 Hz) and 6.32 (1H, d, 2.5 Hz). The olefinic protons remain two. The H^1-H^1 COSY experiment (Figure 86) revealed the coupling for these aromatic protons.

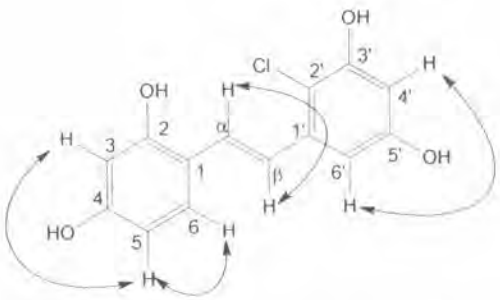

Figure 21: The COSY correlation observed of compound AS-11

3.12. Structural characterization of *cis*-tetra-*O*-methyl oxyresveratrol (AS-12)

Compounds AS-12 was oil obtained from a photo reaction of AS-6. The UV spectrum (Figure 85) showed a maximal absorption at λ_{max} 280 nm, and exhibited IR bands (Figure 86) at 3204 (OH) and 1519 (aromatic ring) cm^{-1}. The EI mass spectrum (Figure 87) revealed a $[M+Na]^+$ ion at *m/z* 323, consistent with the molecular formula $C_{18}H_{20}O_4$. Other significant peaks were found at *m/z* 317. The high resolution mass spectroscopy revealed *m/z* at 323.1268 (323.1262 calculated for $C_{18}H_{20}O_4Na$)

Compound AS-12 was confirmed of the *cis* configuration by the coupling constant (12.1 Hz) of the olefinic protons at δ 6.61 and 6.46. The presence of four methoxyl groups was revealed by the ^1H NMR signals at δ 3.79 (3H, s), 3.77 (3H, s) and 3.63 (6H, s). Six aromatic protons appeared at δ 7.14 (1H, d, 8.4), 6.43 (2H, br s), 6.42 (1H, br s), 6.25 (1H, dd, 8.4, 2.4) and 6.27 (1H, t, 2.1). The ^{13}C NMR spectrum showed the methoxyl carbons at δ 55.8, 55.7 and 55.5. The H^1-H^1 COSY experiment (Figure 92) revealed the coupling for these aromatic protons.

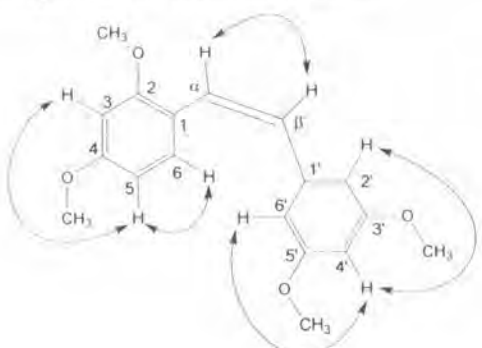

Figure 22: The COSY correlation observed of compound AS-12

3.13. Structural characterization of tetra-*O*-methyl dihidrooxyresveratrol (AS-13)

Compounds AS-13 was obtained as oil. The UV spectrum (Figure 94) showed a maximal absorption at λ_{max} 278 nm, and exhibited IR bands (Figure 95) at 1588 cm^{-1}. The EI mass spectrum (Figure 96) revealed a $[M]^+$ ion at *m/z* 302, consistent with the molecular formula $C_{18}H_{22}O_4$. Other significant peaks were found at *m/z* 151 ($C_9H_{11}O_2$). The high resolution mass spectroscopy revealed *m/z* at 303.1592 (303.1597 calculated for $C_{18}H_{23}O_4$)

Compound AS-13 showed the presence of four methylene protons at δ 2.79 (4H, m) and two methylene carbons at δ 36.8 and 31.6. The ^{13}C NMR revealed the presence of methoxyl proton at 3.76 (6H, s), 3.78 (3H, s), 3.80 (3H, s) and carbons at δ 55.4 and and 55.3.

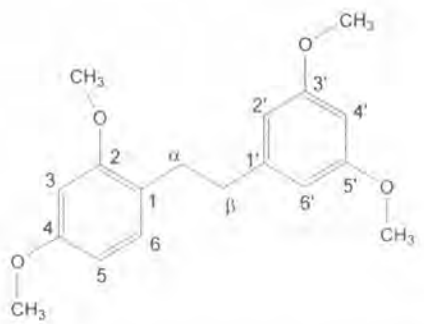

Figure 23: Structure of compound AS-13

4. Tyrosinase activity

4.1. Screening for the tyrosinase inhibitory activity

All of the oxyresverarol derivatives prepared in this study were evaluated for tyrosinase inhibitory activity initially at the concentration of 100 μM, using oxyresveratrol and kojic acid as positive controls. Statistic calculation was performed by Microsoft® Office Excel 2003 and the graph was plotted by SigmaPlot 2000 version 6.10. It was found that only dihydrooxyresveratrol (AS-7) showed more than 80% inhibition, and therefore the compound was further analyzed to determine the IC_{50} value (Table 18). It appeared that dihydrooxyresveratrol (AS-7) was a stronger inhibitor than both oxyresveratrol and kojic acid, both of which are well-known tyrosinase inhibitors, in

terms of the IC_{50} values. AS-7, similar to oxyresveratrol and kojic acid, inhibited the enzyme in a dose-dependent manner in both the substrate-inhibitor pre-incubation and enzyme-inhibitor pre-incubation methods (Figures 23 and 24).

Table 18: Effects on each tyrosinase activity are represented as inhibition %, Mean ± S.E. of three independent tests at 100 μM.

	% inhibition			Mean % inhibition	IC^{*}_{50} (μM)	IC^{**}_{50} (μM)
AS-1	-14.05	-24.88	-20.00	-19.64±3.13	>135	>135
AS-2	-51.23	-30.77	-32.16	-38.05±6.60	>135	>135
AS-3	4.02	6.77	1.87	4.22±1.42	>135	>135
AS-4	-3.61	5.06	-4.69	-1.08±3.08	>135	>135
AS-5	4.75	3.12	-6.63	0.41±3.55	>135	>135
AS-6	3.10	-5.27	-3.99	-2.05±2.60	>135	>135
AS-7	95.38	97.40	96.20	$96.33\pm0.59^{\alpha}$	1.64	1.29
AS-8	-9.75	-7.11	-11.81	-9.56±1.36	>135	>135
AS-9	-1.25	-6.39	-13.50	-7.05±3.55	>135	>135
AS-10	6.29	6.49	1.47	4.75±1.64	>135	>135
AS-11	31.18	31.15	32.52	$31.62\pm0.45^{\alpha}$	>135	>135
AS-12	0.22	-2.10	-6.30	-2.73±1.91	>135	>135
AS-13	4.28	6.52	-3.90	2.30±3.17	>135	>135
Kojic acid	43.22	41.48	38.52	$41.07\pm1.37^{\beta}$	133.40	145.03
Oxyresveratrol	85.09	83.42	81.89	$83.47\pm0.92^{\alpha}$	12.73	9.65

$^{\alpha}$ Significant difference from the control is $p < 0.001$

$^{\beta}$ Significant difference from the control is $p < 0.005$

* substrate-inhibitor pre-incubation method

** enzyme-inhibitor pre-incubation method

(The value was calculated by Microsoft® Office Excel 2003)

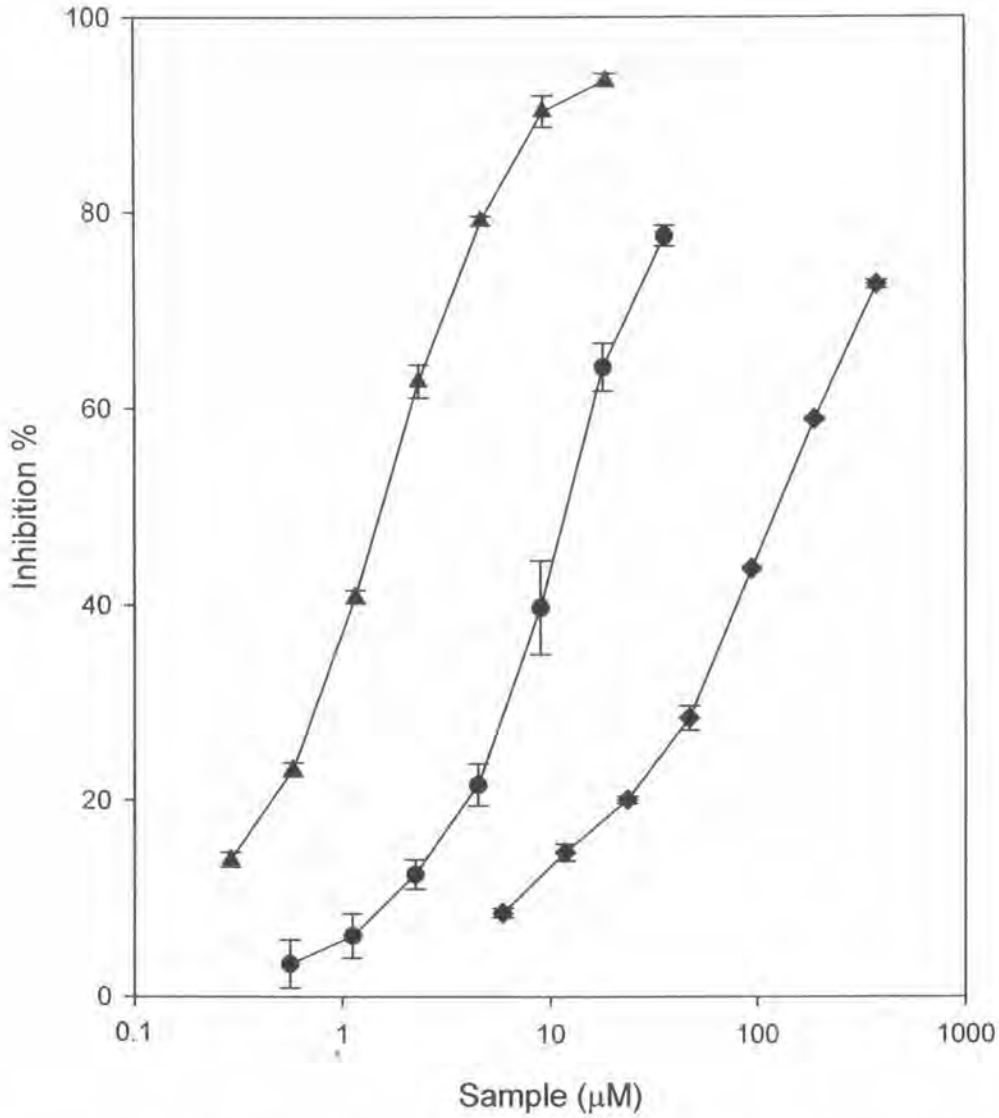

Figure 24: Dose-dependent inhibitory effects on mushroom tyrosinase by oxyresveratrol (circle, ●) , dihydrooxyresveratrol (triangle, ▲) and kojic acid (diamond, ◆). Samples shown are oxyresveratrol (circle, ●) Dihydrooxyresveratrol (triangle, ▲) and kojic acid (diamond, ◆) (substrate-inhibitor pre-incubation method) (Graph was plotted by SigmaPlot 2000 version 6.10)

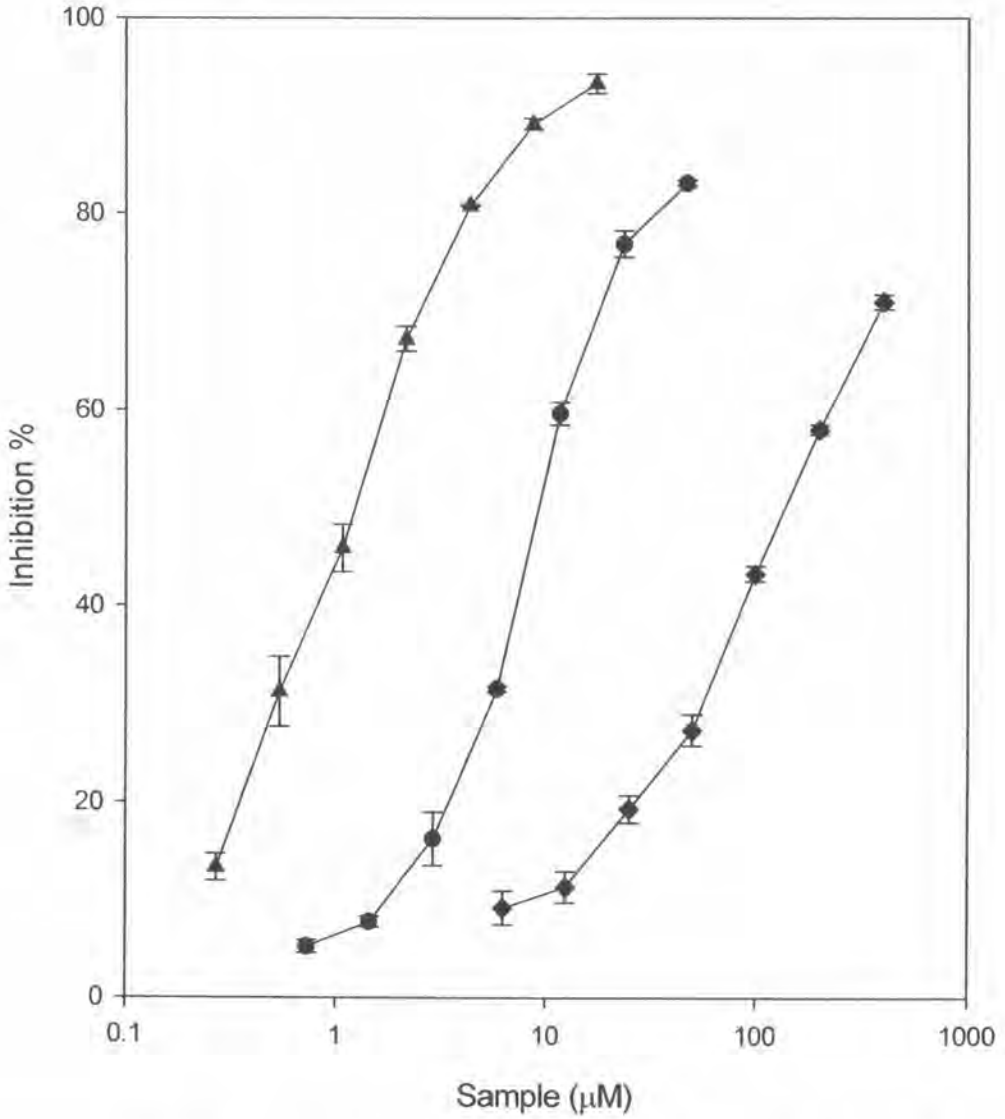

Figure 25: Dose-dependent inhibitory effects on mushroom tyrosinase by oxyresveratrol (circle, ●) , dihydrooxyresveratrol (triangle, ▲) and kojic acid (diamond, ◆). Samples shown are oxyresveratrol (circle, ●) Dihydroxy-oxyresveratrol (triangle, ▲) and kojic acid (diamond, ◆). (enzyme-inhibitor pre-incubation method) (Graph was plotted by SigmaPlot 2000 version 6.10)

4.2. Enzyme kinetics

To determine the mechanism of tyrosinase inhibition by dihydrooxyresveratrol (AS-7) , a kinetic study of the enzyme in the presence of the compound was conducted and then analyzed in comparison with oxyresveratrol and kojic acid. The results of this study are shown in Tables 20, 22, and 24, and Figures 25, 26 and 27. From Table 20 and figure 25, it can be seen that oxyresveratrol did not affect K_m, but decreased V_{max} of the enzyme, and therefore was a non-competitive inhibitor of tyrosinase. This is consistent with earlier reports (Shin *et al.*, 1998a). Similarly, dihydrooxyresveratrol was also a non-competitive inhibitor as evident from the unchanged K_m and decreased V_{max} of the enzyme in the presence of the compound. By comparing K_i values of oxyresveratrol and dihydrooxyresveratrol, the value of dihydrooxyresveratrol was about 4-fold higher in affinity for binding the enzyme than did the parent compound oxyresveratrol, suggesting that the stronger activity was related to the stronger binding. Finally, kojic acid was found to be an inhibitor of mixed type as both the K_m and V_{max} values of the enzyme were affected. The nature of mixed type inhibition of kojic acid was previously reported (Chen *et al.*, 1991; Kim *et al.*, 2002).

Table 19: The 1/V value of oxyresveratrol with variety of substrate concentrations

1/[S]	control	S.E.	Oxy 46	S.E.	Oxy 92	S.E.
8.0000	34.0900	3.9416	48.9811	8.0648	57.8129	21.6502
6.0000	26.2250	3.1025	37.5875	6.8163	44.7385	17.1559
4.0000	20.2210	2.4622	30.1904	7.0899	36.3139	12.7327
2.0000	11.8630	1.6351	17.9211	4.1046	21.8117	6.8590
1.0000	N/A	N/A	11.2085	3.1166	12.4896	4.1210

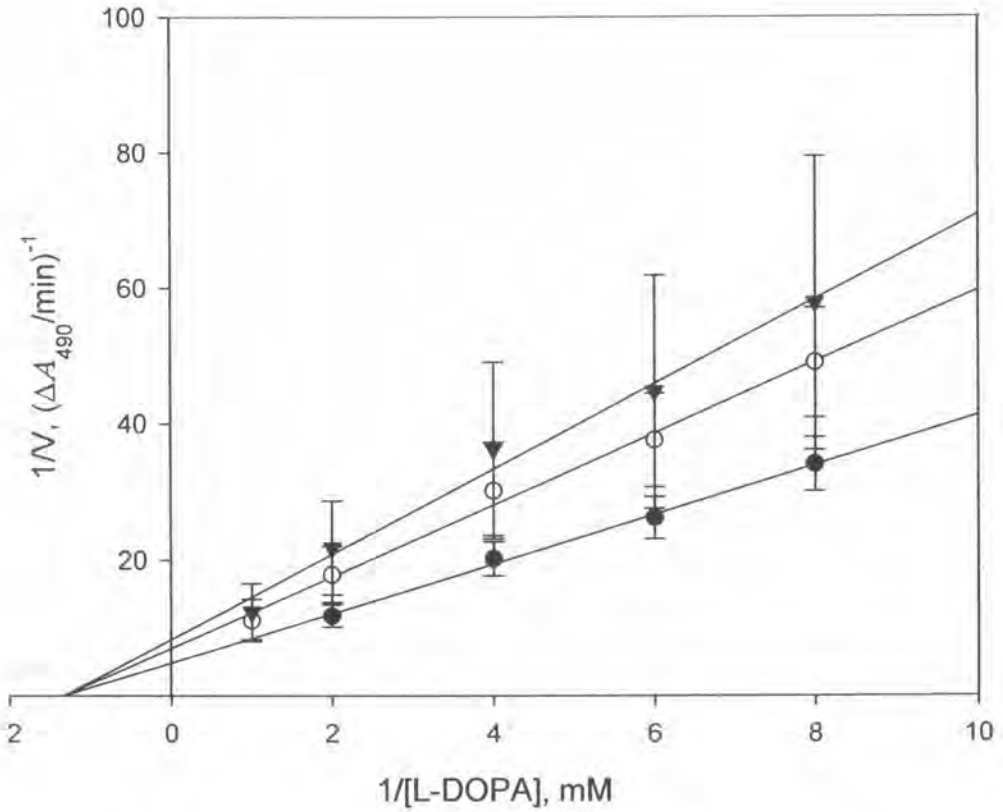

Figure 26: Lineweaver-Burk plot of mushroom tyrosinase in the presence of Oxyresveratrol. Data were obtained as mean values of 1/V, inverse of the increase of absorbance at the wavelength 490 nm per min (ΔA_{492}/min), with different concentrations of L-DOPA as a substrate. Inhibitors of the enzyme were oxyresveratrol with 18.4 μM (triangle, ▼), 9.2 μM (circle, ○) and no oxyresveratrol (circle, ●) (Graph was plotted by SigmaPlot 2000 version 6.10)

Table 20: Kinetic parameters of mushroom tyrosinase in the presence of Oxyresveratrol

Inhibitor	Dose (μM)	K_m (M)	Vmax (ΔA_{492}/min)	K_i (M)
None		0.7×10^{-3}	2.03×10^{-1}	
Oxyresveratrol	9.2	0.7×10^{-3}	1.40×10^{-1}	20.44×10^{-6}
Oxyresveratrol	18.4	0.7×10^{-3}	1.18×10^{-1}	25.54×10^{-6}

Table 21: The 1/V value of AS-7 dihydrooxyreveratrol with variety of substrate concentrations

1/[S]	control	SE	AS-7 6 μM	SE	AS-7 12 μM	SE
8.0000	34.0900	3.9416	42.0300	8.8152	44.7800	11.4379
6.0000	26.2250	3.1025	31.6970	5.2461	36.7650	7.1953
4.0000	20.2210	2.4622	24.8200	4.0924	26.8770	5.4086
2.0000	11.8630	1.6351	14.7390	2.3681	15.6500	3.3329

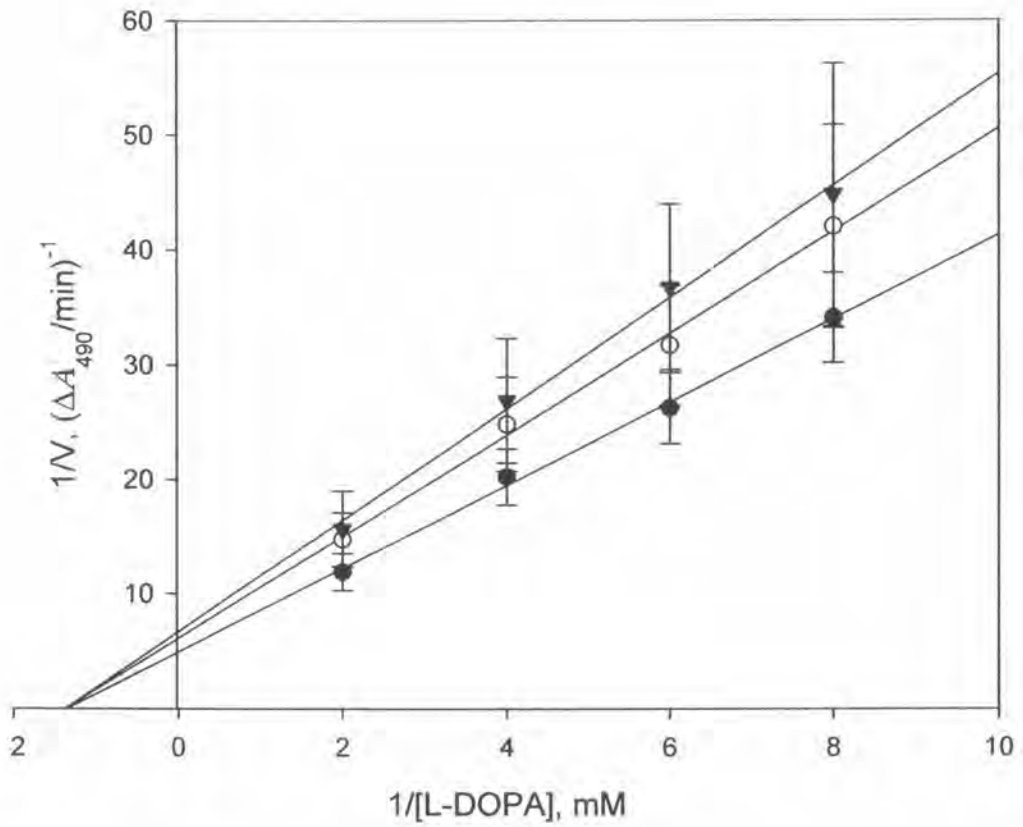

Figure 27: Lineweaver-Burk plot of mushroom tyrosinase in the presence of AS-7. Data were obtained as mean values of 1/V, inverse of the increase of absorbance at the wavelength 490 nm per min (ΔA_{492}/min), with different concentrations of L-DOPA as a substrate. Inhibitors of the enzyme were dihydro-oxyresveratrol with 2.4 μM (triangle, ▼), 1.2 μM (circle, O) and no dihydro-oxyresveratrol (circle, ●) (Graph was plotted by SigmaPlot 2000 version 6.10)

Table 22: Kinetic parameters of mushroom tyrosinase in the presence of dihydrooxyresveratrol

Inhibitor	Dose (μM)	K_m (M)	Vmax (ΔA_{492}/min)	K_i (M)
None		0.7×10^{-3}	2.03×10^{-1}	
Dihydro-oxyresveratrol	1.2	0.7×10^{-3}	1.63×10^{-1}	4.89×10^{-6}
Dihydro-oxyresveratrol	2.4	0.7×10^{-3}	1.49×10^{-1}	6.62×10^{-6}

Table 23: The 1/V value of kojic acid with variety of substrate concentrations

1/[S]	control	Kojic acid 350	Kojic acid 700
8.0000	42.7493	102.0304	146.9983
6.0000	32.9680	74.4214	121.1593
4.0000	25.6501	57.4633	82.4226
2.0000	15.5039	33.0681	49.4091
1.0000	9.7689	19.6583	33.3313

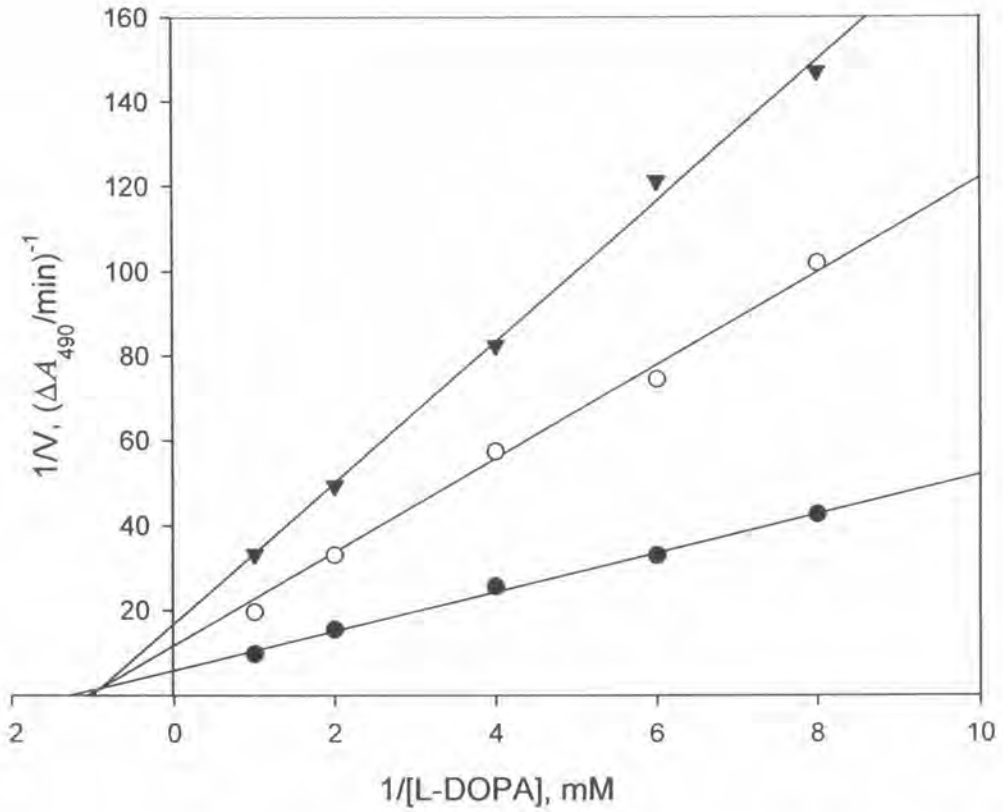

Figure 28: Lineweaver-Burk plot of mushroom tyrosinase in the presence of kojic acid. Data were obtained as mean values of 1/V, inverse of the increase of absorbance at the wavelength 490 nm per min (ΔA_{492}/min), with different concentrations of L-DOPA as a substrate. Inhibitors of the enzyme were kojic acid with 2.4 μM (triangle, ▼), 1.2 μM (circle, ○) and no kojic acid (circle, ●) (Graph was plotted by SigmaPlot 2000 version 6.10)

Table 24: Kinetic parameters of mushroom tyrosinase in the presence of Kojic acid

Inhibitor	Dose (μM)	K_m (M)	Vmax (ΔA_{492}/min)	K_i (M)
None		0.64×10^{-3}	1.44×10^{-1}	
Kojic acid	70	0.88×10^{-3}	8.1×10^{-2}	90×10^{-6}
Kojic acid	140	0.97×10^{-3}	5.8×10^{-2}	94×10^{-6}

Oxyresveratrol was a noncompetitive inhibitor of mushroom tyrosinase enzyme with the K_i = 7.56 x 10^{-7} and 37.78 x 10^{-6} at 9.2 and 18.4 μM respectively. AS-7 or dihydrooxyresveratrol was a noncompetitive inhibitor with the K_i = 4.92 x 10^{-6} and 6.50 x 10^{-6} at the concentration 1.2 and 2.4 μM respectively. Kojic acid showed mixed-type inhibitor at the K_i= 127.65 x 10^{-6} and 4.41 x 10^{-6} at the concentrations of 70 and 140 μM.

5. Cytotoxicity assay

Evaluation of cytotoxicty of the *O*-methylated derivatives was performed in three human cancer cell lines: KB, BC and NCI-H187, and the results are summarized in Table 25. Correlation was found between the number of methoxy groups and cytotoxicity. *cis*-Tetra-*O*-methylated oxyresveratrol (AS-12) was the most potent compound, being stronger than the positive control ellipticine.

Table 25: Cytotoxicity activity of compounds against KB, BC, NCI-H187 cell lines

Compounds	Cell lines IC_{50} μg/ml		
	KB	BC	NCI-H 187
AS-6	2.6	1.7	2.4
AS-7	>20	>20	>20
AS-8	1.48	2.94	2.98
AS-9	4.54	3.78	9.12
AS-10	>20	17.20	>20
AS-12	0.1	0.3	0.132
AS-13	>20	7.63	>20
Oxyreveratrol	12.58	5.55	>20
Ellipticine	0.75	0.61	0.47
Doxyrubicin	0.17	0.24	0.031

The *cis*-form of tetra-methylated oxyresveratrol is more potent than *trans* and also partial-methylated of *trans*-form. It is known that methoxy groups are crucial for cytotoxic activity and that *cis* conformation raises the potency of activity (Cushman *et al.*, 1992). Combretastatins are examples of naturally occurring *cis*-polymethoxystilbenes having cytotoxicity (Cushman, *et al.*, 1991). AS-7, dihydrooxyresveratrol was inactive against all cell lines which confirmed the safety of the compounds.